

## Validation and Improvement Suggestions for MICE Experimental Hall Modelling

Prepared by Chris Riley and Klaus Höffer

### Introduction

The purpose of this report is to investigate the RAL/University of Sheffield models for the MICE Experimental Hall. The work is divided into 5 sections:

1. Comparison of results from a free space finite element model with fields computed using Biot-Savart expressions
2. Investigation of the influence of ferromagnetic components in the model on the results
3. Investigation of the sensitivity to material properties in the ferromagnetic components
4. Accuracy of the model and the effect of element order
5. Extraction of fields from the main model to investigate detailed substructure models.

A second report on substructuring, "A further investigation of substructure and simplification modelling for the RAL MICE Hall" has also been prepared to investigate more generic advice on substructure models.

### Item 1 - Comparison of fields in free space

Before determining the validity of the MICE Hall model and suggesting any improvements, the effect of using the finite element method is investigated. The field from the solenoids used in MICE can be evaluated to an accuracy of about 1 part in 100 million using the Biot-Savart expressions implemented on a digital computer. However, the finite element mesh used for the MICE Hall will not allow this accuracy because of

- Numerical issues associated using low order polynomial representation of the fields in the elements
- Numerical issues associated with solution of the equations
- Truncation of infinite space by a finite meshed area

The aim of this section of the report is to obtain some idea about how using finite elements has affected accuracy from a comparison of fields in a free space finite element model (where all components have the material properties of air) with Biot-Savart calculations.

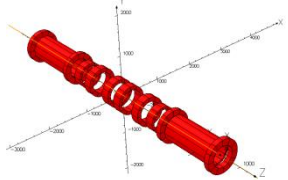
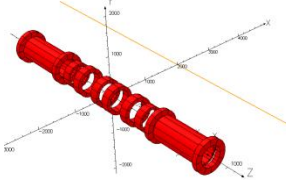
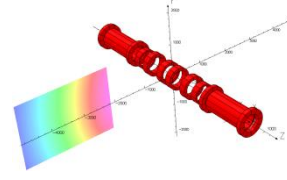
The investigation has been done with Model 91 which has 15.6 Million active elements; all elements are quadratic. The results presented are the field along the solenoid axis, the field along a line 2000 mm from the solenoid axis in the same horizontal plane and the field on a Cartesian patch orthogonal to the axis where there will be significant return flux. Although graphical results for these are presented (figures 1 through 3), it is actually more instructive to compare integral values, as shown in Table 1.

The accuracy of the field on axis computed by the finite element mesh is extremely high. This is to be expected as these fields are being recovered in reduced magnetic potential regions where the finite elements are only representing the magnetization field. The magnetization field should be identically zero since all magnetic components have been set to air properties. The very small error results from the numerical issues outlined above.

However, in other areas of the model, the accuracy is in the order of about 0.2%. These fields are recovered in total potential regions where the finite elements are representing the total field. The inaccuracy is primarily due to the truncation of infinite space by the boundary of the mesh which implies images of the model space.

It would be expected that the difference between the finite element simulation and the Biot-Savart results would increase further closer to the model boundary.

**Table 1: Comparison of nodal and integral fields**

			
	$\int_{z=-7500}^{z=+1500} B_z dz$ $x=0$ $y=0$	$\int_{z=-7500}^{z=+1500} B_z dz$ $x=2000$ $y=0$	Flux through a patch in XY-plane @ Z=-3000, X: -4800 to -2000, Y: -1000 to +1000 $\int B_z dx dy$
Biot-Savart coils (integral fields)	24173.37011 T-mm	-51.6616 T-mm	-23083.5364 T-mm <sup>2</sup>
Finite Element mesh (nodal fields)	24173.11681 T-mm	-51.7435 T-mm	-23133.1985 T-mm <sup>2</sup>
Percent error	0.001 %	0.16 %	0.21 %

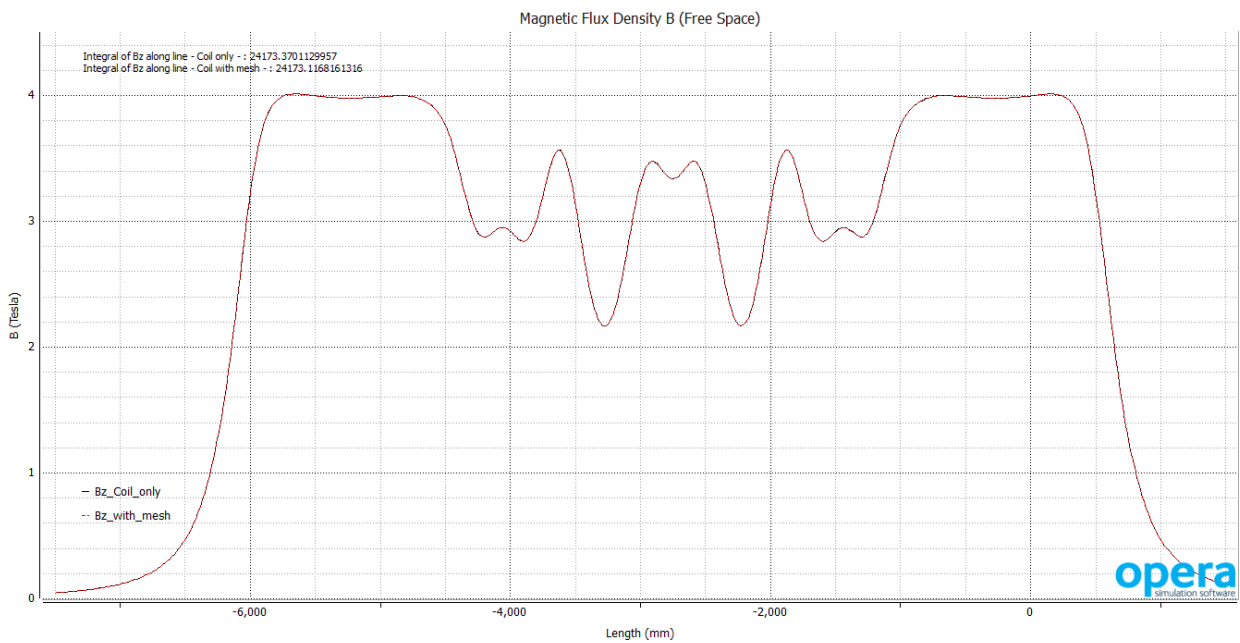


**Figure 1: Z-directed lines at X = 0, Y = 0**

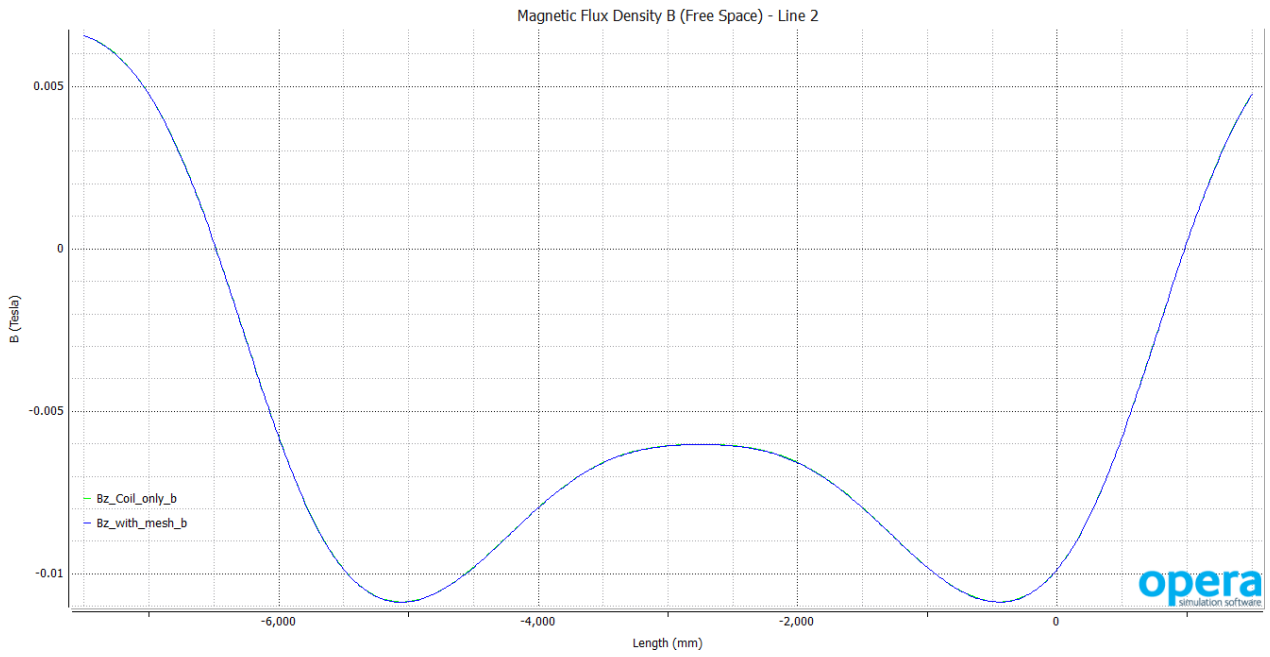


Figure 2: Z-directed lines at X = +2000, Y = 0

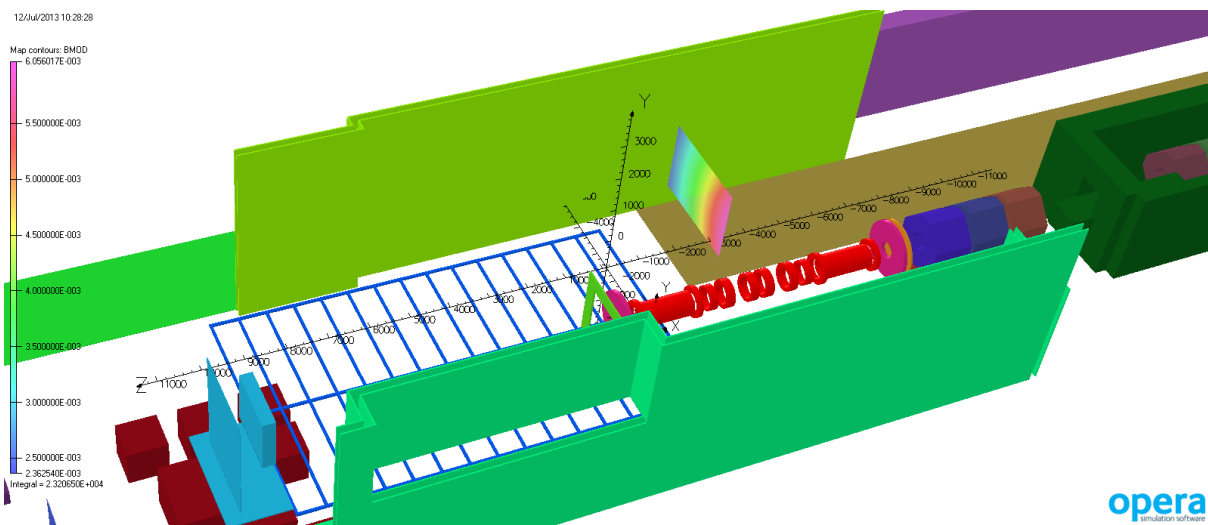


Figure 3: Position of patch 1 (XY) in the model space

## Item 2 - Adding ferromagnetic components to the model

The next investigation is to determine the significance of the ferromagnetic components included in the model in determining the overall accuracy of the simulation. There are 48 individual material names used in Model 91 (although some of these are assigned permeability = 1 and are only included for visualization purposes). However, there are still 31 separate ferromagnetic components. Adding each one individually would be very time consuming (and probably not all that instructive!). Consequently, components have been added in groups that have similar locations in the model.

Starting from the model where all components have material properties of air, ferromagnetic components were added in the following order.

**Table 2: Overview of cases**

Case name	
MAT_0	all air
MAT_1	4 "lenses" added (EMR, uTOFc, VP)
MAT_2	as MAT_1, added side walls + floorweb (NSW, SSW, Floorweb)
MAT_3	as MAT_2, added cellar steel (Cellar)
MAT_4	as MAT_3, added beam dump (Beam_Dump)
MAT_5	as MAT_4, added the shield around Q4– Q6 (DSA_RS)
MAT_6	as MAT_5, added quadrupoles Q7– Q9 (Q7, Q8, Q9)
MAT_all	includes all ferromagnetic parts in model 91

Figures 4 through 11 show these different models

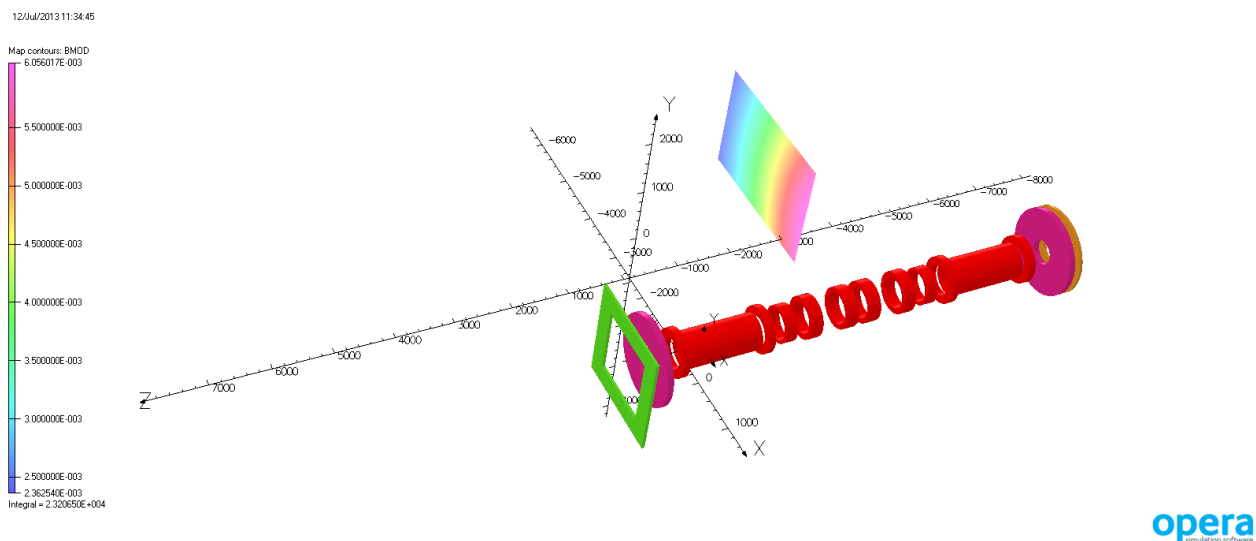


**Figure 4: Ferromagnetic parts in MAT\_1, 4 "lenses" added**

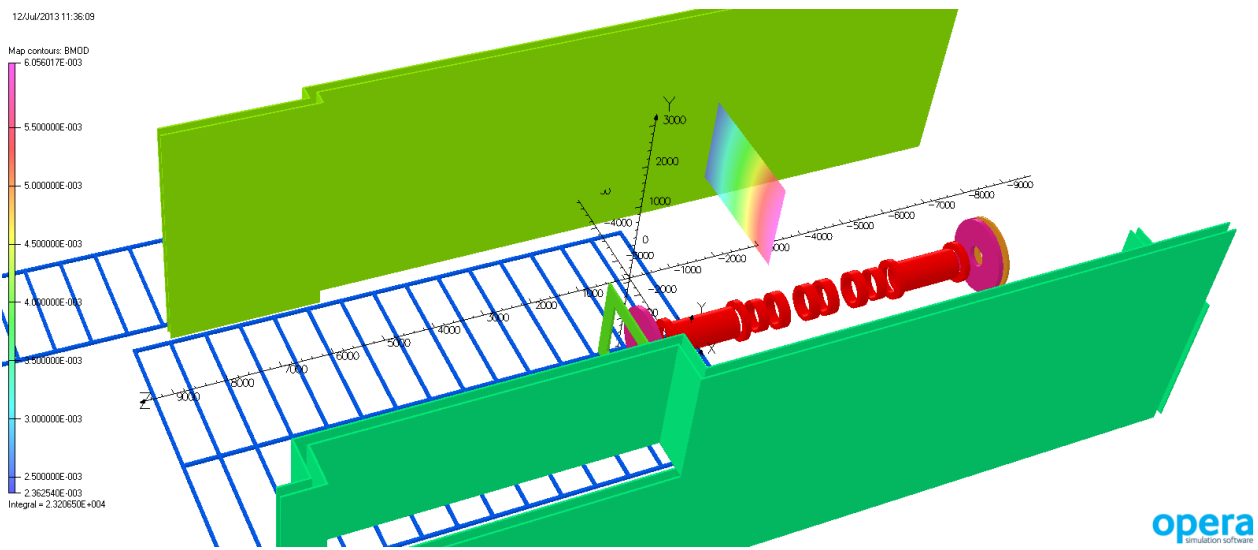


Figure 5: Ferromagnetic parts in MAT\_2, side walls + floorweb added

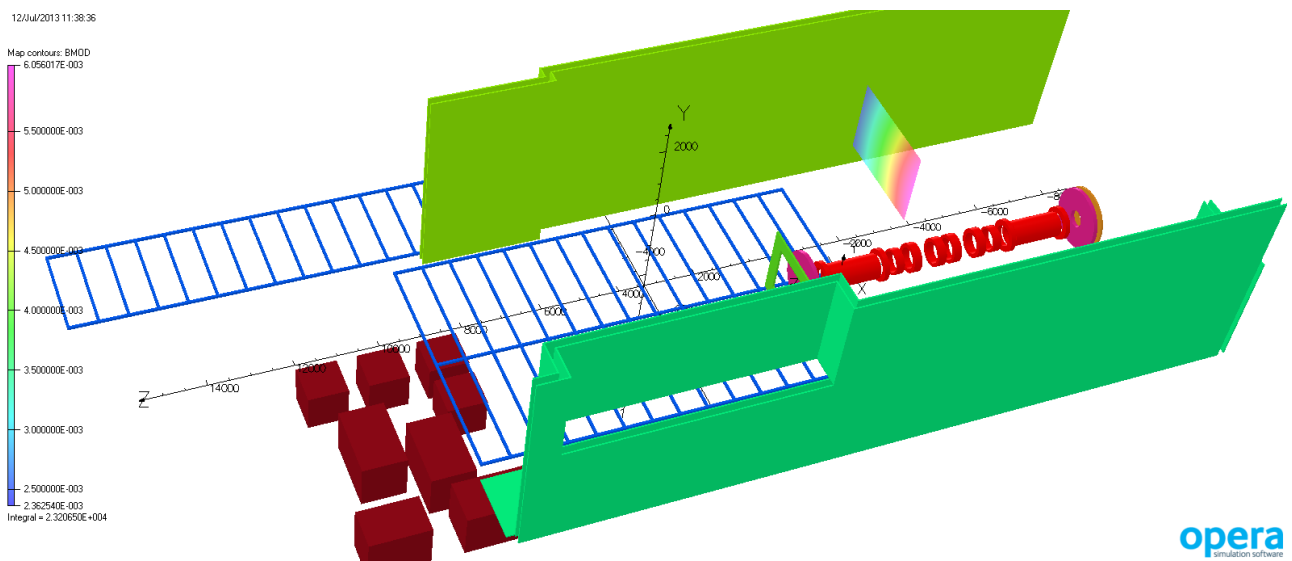


Figure 6: Ferromagnetic parts in MAT\_3, cellular steel added

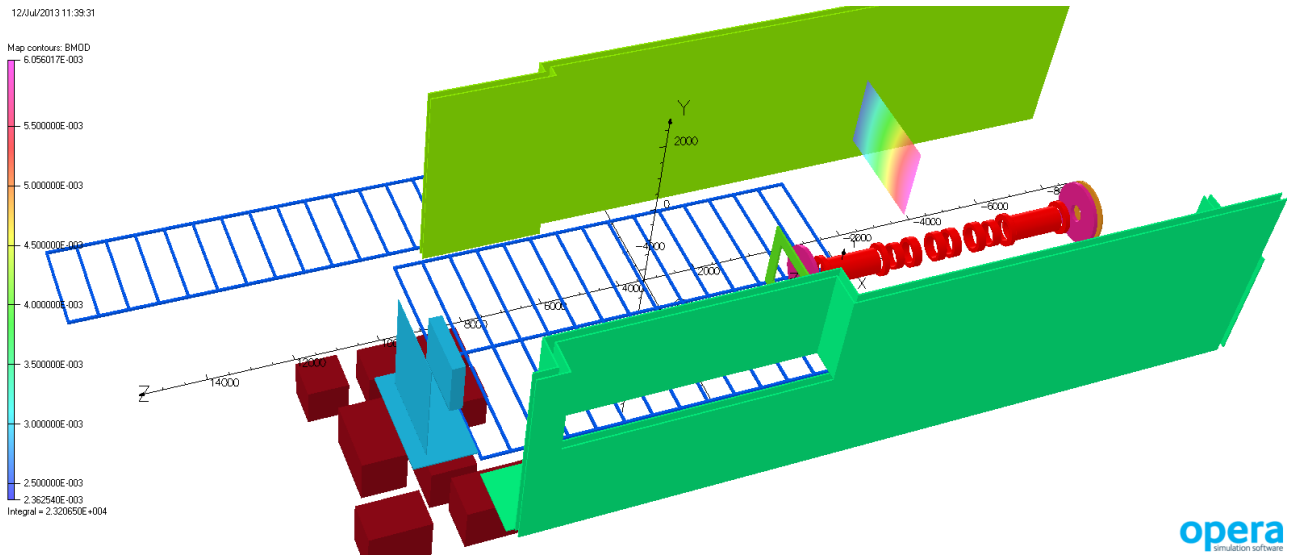


Figure 7: Ferromagnetic parts in MAT\_4, beam dump added

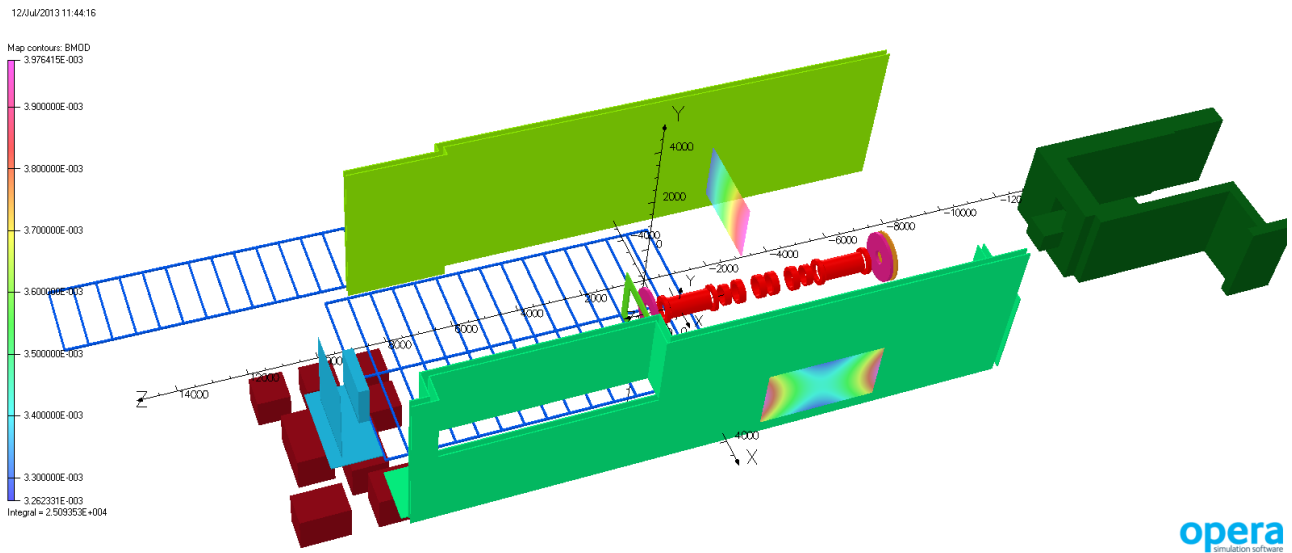


Figure 8: Ferromagnetic parts in MAT\_5, shield around quadrupoles added

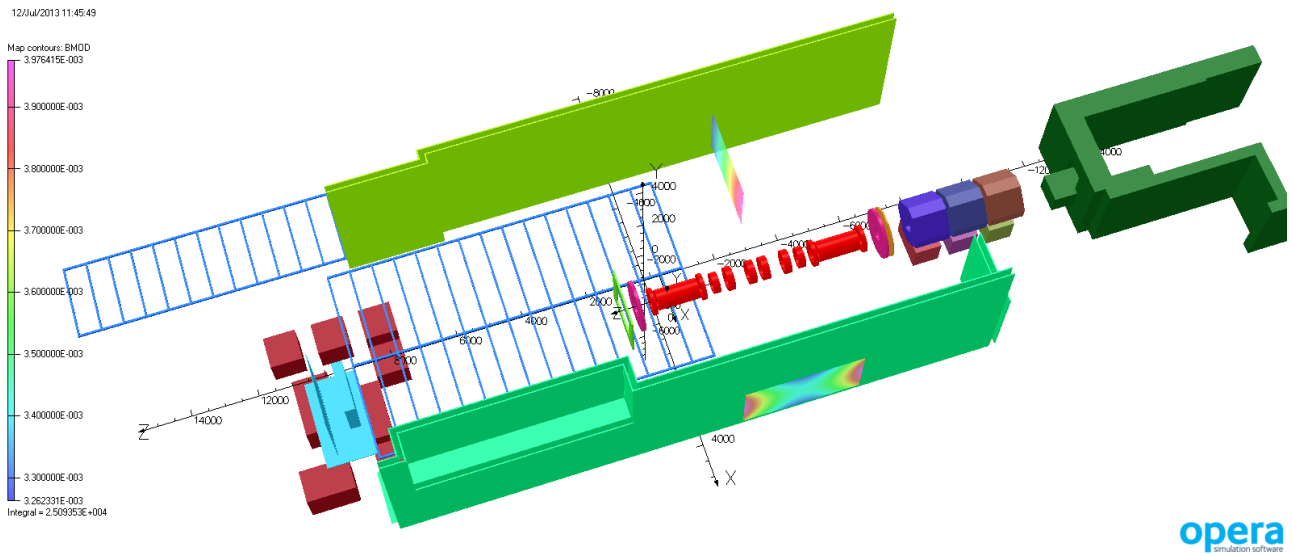


Figure 9: Ferromagnetic parts in MAT\_6, quadrupoles Q7 – Q9 added

12/Jun/2013 12:07:08

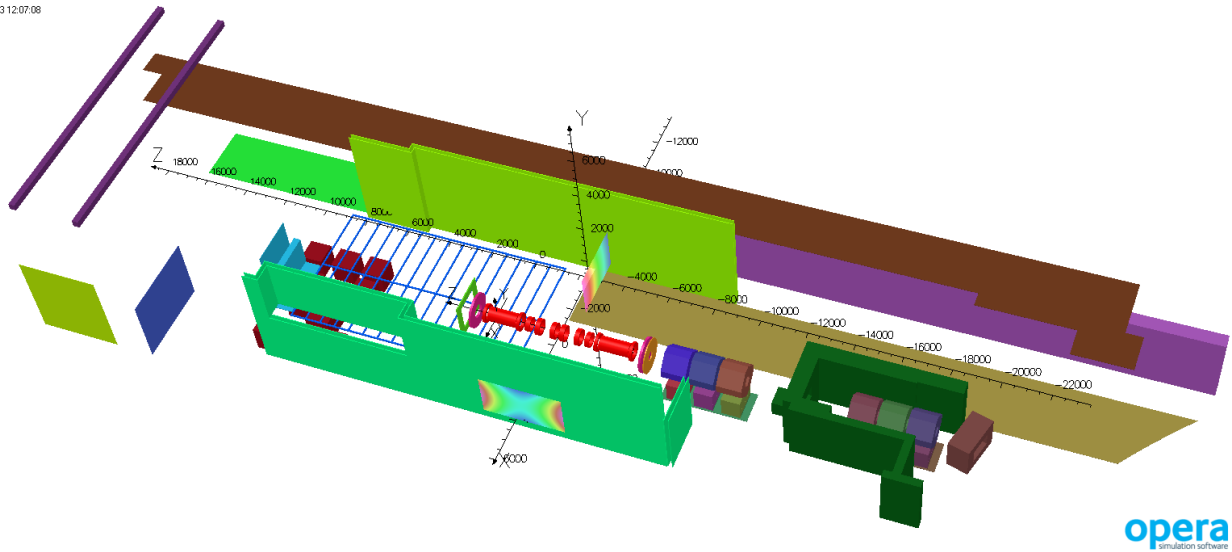
opera  
simulation software

Figure 10: All ferromagnetic parts in model 91 (MAT\_all)

12/Jun/2013 12:08:49

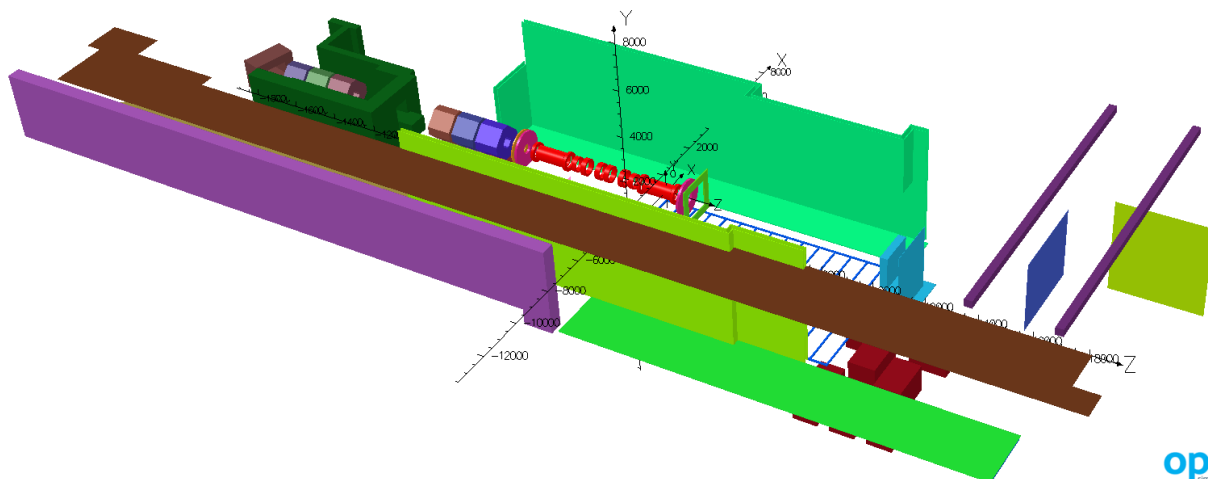
opera  
simulation software

Figure 11: All ferromagnetic parts in model 91 (MAT\_all), different view

Most of these cases we run as restarts from a fully converged nonlinear solution with all materials in place. The 3d Pre-Processor was used to set up these restarts; a typical structure of a script is shown below. As stated above, Model 91 features a total of 48 material names; in the example most of them have been omitted to improve readability.

```
/ Opera-3d Pre-Processor  
/ Opera 16 [Build 29934] (x64)  
/ Started: 17/Jun/2013 11:06:09  
/ Node: PREC01. Processor: Intel64/x64. System: Windows 7 (Service Pack 1)
```

```
SOLV OPTI=DEFA
$STRI ANLT TOSCA|SOLV PROG=TOSCA,TYPE=MAGN, DRSCALE=YES,
SOLV FILE='KJH_model91_allMat_mu_original__MAT1.op3' OPTI=RESTART CASE=1
  RESTART in PRE
  *

MATE NAME=BEAM_DUMP_CONCRETE TYPE=LINE ANIS=ISOT
MATE MUX=1 HCZ=0
MATE NAME=BEAM_DUMP_STEEL TYPE=LINE ANIS=ISOT
MATE MUX=1 HCZ=0
...
...
MATE NAME=EAST_WALL_CONCRETE TYPE=LINE ANIS=ISOT
MATE MUX=1 HCZ=0

MATE NAME=EMR_Steel TYPE=NONL ANIS=ISOT
MATE BHX='RAL_MildSteel.bh'

MATE NAME=FLOORWEB_STEEL TYPE=LINE ANIS=ISOT
MATE MUX=1 HCZ=0
MATE NAME=FLOOR_CONCRETE_LOWER TYPE=LINE ANIS=ISOT
MATE MUX=1 HCZ=0
...
...
MATE NAME=SWDB_STEEL TYPE=LINE ANIS=ISOT
MATE MUX=1 HCZ=0
MATE NAME=TRFP_FLOORPLATE_STEEL TYPE=LINE ANIS=ISOT
MATE MUX=1 HCZ=0

MATE NAME=uTOFc_Steel TYPE=NONL ANIS=ISOT
MATE BHX='RAL_TenTen.bh'
MATE NAME=VP_Steel TYPE=NONL ANIS=ISOT
MATE BHX='RAL_TenTen.bh'

MATE NAME=WEST_WALL_CONCRETE TYPE=LINE ANIS=ISOT
MATE MUX=1 HCZ=0
SETT RHS=ADAP
QUIT
```

To characterise the implications of adding ferromagnetic materials, the magnetic flux density has been calculated on 3 patches. The first patch is the same as in Item 1 (XY plane at Z=-3000), the second is behind the NSW wall (YZ plane at X=-5300) as shown in figure 12, and the third is behind the SSW wall (YZ plane at X=+3920) as shown in figure 13.

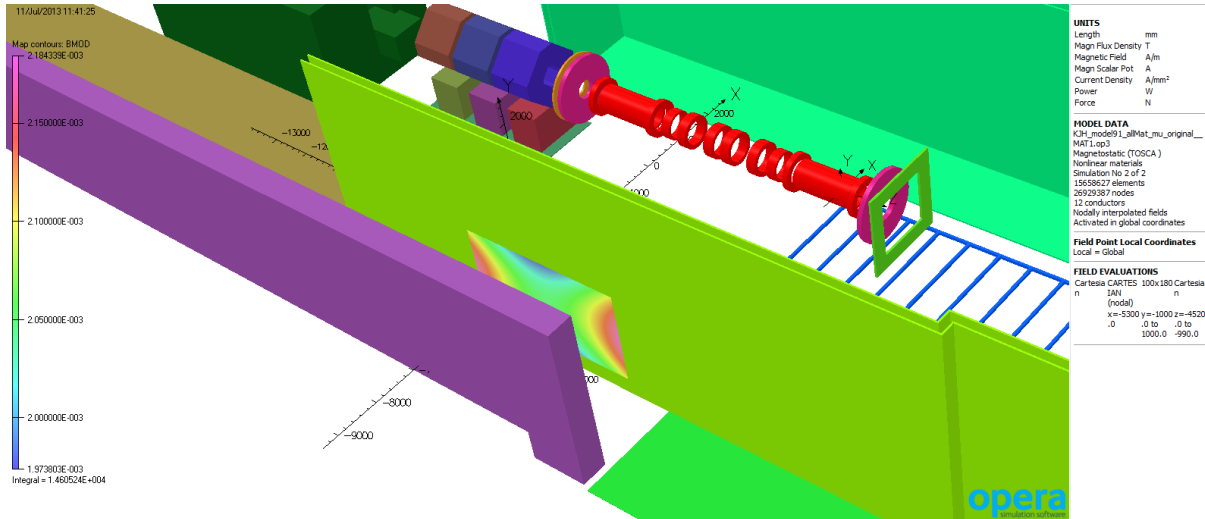


Figure 12: Position of patch 2 behind NS W

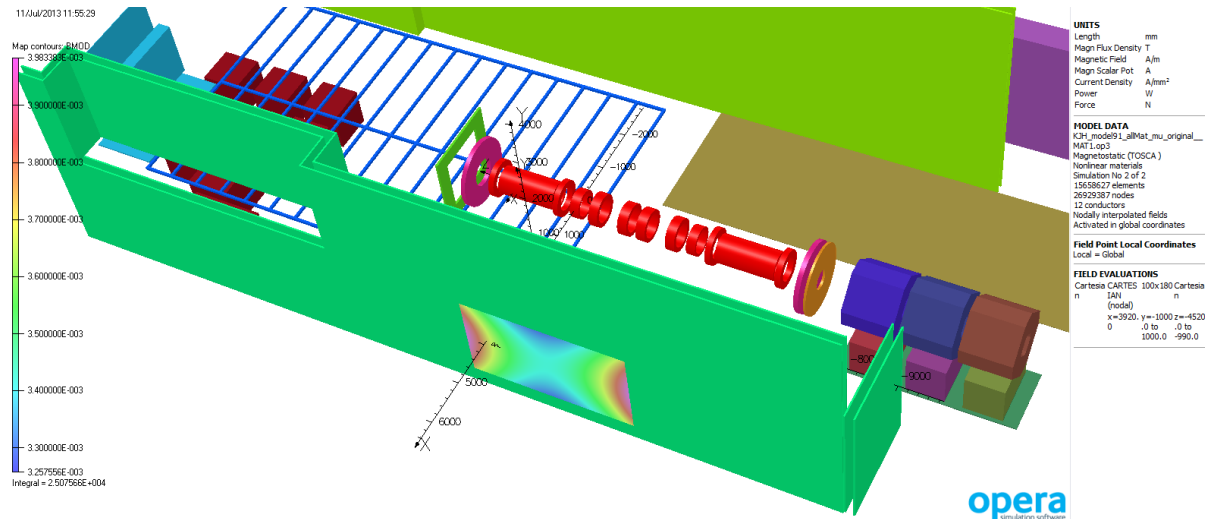


Figure 13: Position of patch 3 behind SS W

Patch 1 intersects the return path of the flux, where the field is directed in negative Z. Therefore it was sufficient to integrate  $-B_z$  to obtain a representative number. On patches 2 and 3 only little flux is intersecting; the direction of the field is nearly parallel to the patch. Therefore the absolute value of the flux density normal to the patch was integrated:

$$\text{MAP FILE=TEMP COMPONENT=ABS (BX*NX+BY*NY+BZ*NZ)}$$

In addition, the values for B\_min and B\_max were recorded for each of the three patches. These results are shown in tables 3 and 4.

Table 3: Integrals on patches in [T · mm<sup>2</sup>]

Integrals on patches	Patch 1 (XY)	Patch 2 (YZ)	Patch 3 (YZ)
model91_allMat_mu_1.op3	23133.2	4543.564	8117.124
model91_allMat_mu_original_MAT1.op3	22879.38	4534.942	7977.290
model91_allMat_mu_original_MAT2.op3	14022.02	1120.718	189.2561
model91_allMat_mu_original_MAT3.op3	14021.47	1115.108	183.6692

model91_allMat_mu_original__MAT4.op3	14020.24	1111.936	182.2095
model91_allMat_mu_original__MAT5.op3	13997.83	1149.024	238.8757
model91_allMat_mu_original__MAT6.op3	13368.59	1408.696	526.1588
model91_allMat_mu_original.op3	11779.61	2588.172	670.6671

Table 4: Minimum and maximum values of B on patches in [Gauss]

	Patch1 BZmin	Patch1 BZmax	Patch2 Bmin	Patch2 Bmax	Patch3 Bmin	Patch3 Bmax
mu_1.op3	23.5206	60.5199	19.6284	21.6762	32.6233	39.7642
mu_original__MAT1.op3	23.6061	58.6778	19.738	21.8434	32.5756	39.8338
mu_original__MAT2.op3	2.5714	44.7291	1.4174	4.2217	2.2119	2.5599
mu_original__MAT3.op3	2.5708	44.7263	1.4143	4.2129	2.2148	2.5605
mu_original__MAT4.op3	2.5700	44.7248	1.4123	4.2071	2.2113	2.5559
mu_original__MAT5.op3	2.5589	44.6635	1.4224	4.2470	2.1953	2.5643
mu_original__MAT6.op3	2.4808	42.3483	1.5129	4.6617	2.2742	2.8127
mu_original.op3	2.6013	39.6062	3.0449	4.3986	2.2586	2.8156

The results show that the lenses added in MAT\_1 are not very significant – only reducing the return flux in free space (patch 1) by about 1% and having an even smaller effect on the flux at the patches behind the shielding walls. These lenses could probably be omitted from any future model as the differences are in the same order as the error associated with using a finite element representation.

Adding the side walls and floor web has a much more significant effect (MAT\_2). These provide a preferential path for the return flux, thereby reducing the flux on patch 1 by about 40% - although the reduction of the maximum flux density (closest to the solenoids) is only about 25%. This is to be expected as the flux returning through the walls still has to cross a significant air space and a path close to the solenoids will have a similar reluctance.

On patches 2 and 3, the flux and flux density values are much more drastically reduced, as would be expected from the shielding action of the walls. The flux in patch 2 is reduced by more than 75% and the maximum value by more than 80%. On patch 3, the reductions are even greater (about 98% and 97% respectively). This suggests that the NSW wall is less saturated than the SSW wall – which is also to be expected as the SSW wall is closer to the solenoids.

The additions made in MAT\_3 (cellar steel) and MAT\_4 (beam dump) have little effect on the results and the changes observed are below the errors associated with the finite element representation. The MAT\_5 addition (quadrupole shield) has a small effect – further reducing the return flux at patch 1 by about 5%, but actually increasing the flux density behind the side walls (patches 2 and 3). The quadrupole shield will not be saturated and will be a preferential path for the return flux, allowing more Ampere-turns to be available for other parts of the return circuit. Consequently, the side walls will become slightly more saturated making them less effective as shields.

This same effect can be seen more readily with the addition of the Q7 – Q9 quadrupoles (MAT\_6). The flux through patch 2 increases by about 30%, while in patch 3 it more than doubles. However, the increases in the maximum flux density are less extreme (about 10% in both cases).

The final model with all ferromagnetic components shows further significant changes to the results. Return flux through patch 1 is reduced by another 13% but flux through patch 2 increases by nearly 80% and through patch 3 by 20%. The maximum values of flux density are largely unaffected with patch 2 actually reducing by 5%. The most likely component for this increase is the FWN\_floorplate\_steel which again is providing an effective return path. The dipole and quadrupoles Q4 – Q6 are behind the shielding wall and will not be very significant.

This investigation shows that the most significant components are those which substantially affect the return path of the flux. While the results presented have been necessarily reduced, they are representative of important areas in the model where sensitive equipment is potentially to be mounted. The models produced for these studies can be used for field recovery in any other area of the meshed space.

It is probable that the MICE Hall model already contains enough of the significant components for the fields in free space to be accurate within 1 or 2% - remembering of course that all fields may be at least 0.2% of the "all free space" value in error anyway. From Cobham's knowledge of the MICE Experimental Hall, there do not appear to be any major components that have been omitted that will further significantly affect results, although the complete layout drawings have not been available.

## Item 3 – Investigation of material property variations

An investigation has been made into how sensitive the results for the MICE Hall Model 91 are to material properties. In the model, steel components have been either assigned Cobham's 1010 steel magnetic characteristic from the library or the mild steel characteristic from the library. The LINAC wall is made from reinforced concrete and an equivalent curve based on volume fraction has been derived from the mild steel curve. However, it is not known how accurately these curves really represent the actual materials in the MICE Hall.

Consequently, all the models that were presented and discussed under Item 2 were run with modified material properties; the magnetization values of the 3 BH curves were "diluted" by a factor of 90%. The following method was used:

$$B_{new} := \text{dilution factor} \cdot \text{old Magnetisation, } M \text{ (in Tesla)} + \mu_0 \cdot H_{old}$$

and the following COMI shows how this was achieved. Materials that are highly saturated will behave significantly differently with a 10% reduction in material properties – so these experiments will give an indication how sensitive the MICE Hall model is to material property uncertainties.

```

/ Modeller_dilute_RAL.comi
/
$constant #packingf 0.9
/
/ Open input file for reading
$ open 1 RAL_MildSteel.bh read
/ Read the first line into user variable #np
$ read 1 #np #info1 #info2
/ Open output file for writing
$ open 2 RAL_MildSteel_diluted09.bh write
/ Define a string format to space the output
$ format 1 string string=' '
/ Define a floating point format
$ format 2 expo 0
/ Assign format numbers for the output
$ assign 2 1 2 1 2
/
$ write 2 #np #info1 #info2
/
/ first point 0; 0
$ read 1 #b #h
$ write 2 #b #h
/
/ Start a loop from 1 to #np-1
$ do #i 1 #np-1
/ Read #b and #h from input file
$ read 1 #b #h
/
/ Evaluate #b
$if (#info1&&#info2) eq 1 |/SI units
$constant #b (#b-mu0*#h)*#packingf+(mu0*#h)
$else |/CGS
$constant #b (#b-#h)*#packingf+#h
$end if
/
/ Write to output file
$ write 2 #b #h
/ End of loop
$ end do
/ Close files

```

```

$ close 1
$ close 2
/
/ end of comi-script

```

The magnetic field was evaluated with the same method as discussed in the previous item: field integrals, minimum and maximum on 3 patches and the results are presented in tables 5 and 6.

**Table 5: Integrals on patches in [T · mm<sup>2</sup>], diluted materials**

Integrals on patches	Patch 1 (XY)	Patch 2 (YZ)	Patch 3 (YZ)
/			
MAT1_diluted.op3	22880.18	4534.967	7977.702
MAT2_diluted.op3	14113.96	1077.715	187.4631
MAT3_diluted.op3	14112.62	1071.998	183.9351
MAT4_diluted.op3	14112.09	1069.289	182.5235
MAT5_diluted.op3	14088.82	1106.929	219.0933
MAT6_diluted.op3	13459.44	1368.78	493.7205
allMat_diluted.op3	11939.97	2676.976	630.8459

**Table 6: Minimum and maximum values of B on patches in [Gauss], diluted materials**

	Patch1 BZmin	Patch1 BZmax	Patch2 Bmin	Patch2 Bmax	Patch3 Bmin	Patch3 Bmax
/						
MAT1_diluted.op3	23.6059	58.6832	19.7377	21.8428	32.5757	39.8335
MAT2_diluted.op3	2.7300	44.9472	1.5337	4.1129	2.5141	2.8961
MAT3_diluted.op3	2.7292	44.9438	1.5304	4.1036	2.5141	2.8937
MAT4_diluted.op3	2.7287	44.9426	1.5287	4.0990	2.5146	2.8931
MAT5_diluted.op3	2.7166	44.8791	1.5378	4.1388	2.4866	2.8829
MAT6_diluted.op3	2.6352	42.5670	1.6233	4.5525	2.5182	2.9947
allMat_diluted.op3	2.7496	39.9499	3.0742	4.6470	2.4649	2.9494

By comparisons with tables 3 and 4 respectively, it can be readily seen that the results do not have a great sensitivity to the material characteristics. Changes are below 5% in all cases and in many cases much lower. The reduced ability of the side walls to offer a preferential return path can be seen, although they actually now also have less flux to shield so the densities on patches 2 and 3 are actually slightly lower. However, as the side walls are poorer return paths, the flux density values on patch 1 are slightly higher.

Consequently, it is expected that the uncertainty about material properties in surrounding structures should only be of minor concern for the MICE experiment.

## Item 4 – Investigation of mesh quality

In items 1 through 3 and in item 5, all versions of Model 91 were run with the setting that all elements were set to “quadratic”, as had been set by the originators of the models. While this is undoubtedly most accurate, the cost of doing this is to make very large models. In this item, the aim is to find out whether this is really necessary, or whether solution times can be reduced by using linear elements.

Two further models were created. The first of these uses a combination of linear and quadratic elements: all air and all materials with properties of air are set to linear, and all magnetisable materials are set to quadratic. The second model uses linear elements throughout. Table 7 presents important statistics for the simulations. The results presented are the same as those in Items 2 and 3, as shown in tables 8 and 9

**Table 7: Comparison of equation numbers and solution times**

	Linear Elements	Mixed Elements	Quadratic Elements
Number of Elements	15.6 Million	15.6 Million	15.6 Million
Number of Equations	2.64 Million	4.25 Million	21 Million
Nonlinear tolerance	1.0 E-03	1.0 E-03	1.0 E-03
Nonlinear iterations	9	11	10
Used hardware	resource2	prec01	resource2
Solution time	2:45 hours	9:40 hours	58:39 hours

**Table 8: Integrals on patches in [T · mm<sup>2</sup>]**

Integrals on patches	Patch 1 (XY)	Patch 2 (YZ)	Patch 3 (YZ)
mu_original_linearElements.op3	11703.4447	2534.4562	673.8262
mu_original_mixed_Elements.op3	11710.1525	2541.1677	670.2382
mu_original.op3	11779.6056	2588.1721	670.6671

**Table 9: Minimum and maximum values of B on patches in [Gauss]**

	Patch1 BZmin	Patch1 BZmax	Patch2 Bmin	Patch2 Bmax	Patch3 Bmin	Patch3 Bmax
mu_original_linear_Elements.op3	2.5996	39.3038	2.9885	4.3720	2.2798	2.8025
mu_original_mixed_Elements.op3	2.5999	39.3316	2.9986	4.3789	2.2761	2.7996
mu_original_quadratic_Elements.op3	2.6013	39.6062	3.0449	4.3986	2.2586	2.8156

These results show that, on the patches examined, the benefit of using quadratic elements at all is marginal. Changes in results are largely below 1%, while the benefit of the all linear element solution in terms of problem size and corresponding solution time, as shown in table 7, is considerable.

Unfortunately, not all of the models were run on the same hardware due to time constraints, with the *prec01* computer used for the mixed element simulation being a little faster than *resource2* used for the other 2 studies. Nevertheless, as expected, solution times increase more than linearly with equation numbers because:

- iterative sparse matrix solution schemes are approximately dependent to the power of 1.5 with number of equations (assuming same order elements in all cases)
- quadratic element equations contain more terms than linear elements, making a less sparse matrix

## Item 5 - Substructure Modelling in Model 91

The final investigation is of the possibility of using field values from the overall model of MICE Hall as a source field for a detailed substructure model. Model 91 does not include any substructures like cabinets or racks. For a preliminary study to investigate the effects of substructures, the following steps were performed:

1. Solving Model 91 as provided, i.e. with all ferromagnetic materials in place, and no cabinet. (corrected “reducedMildsteel” for Linac Wall, mixed linear/quadratic elements)
2. Retrieved a simplified representative substructure from an old model that had been supplied by RAL in November 2012 (CompStack2\_S4\_1mumetal\_3steel.opc): *rack1.opc*.
3. Inserted *rack1.opc* into Model 91, and performed a Boolean Cutaway operation to trim the “SouthShield” in the model. (do not forget to define #Layer\_th=5)
4. Solving Model 91 with the rack. (corrected “reducedMildsteel” for Linac Wall, mixed linear/quadratic elements)
5. Post-processing the model with the rack (patch in the ZX-plane through the middle of the rack @ Y=-680).

These steps are illustrated in figure 14.

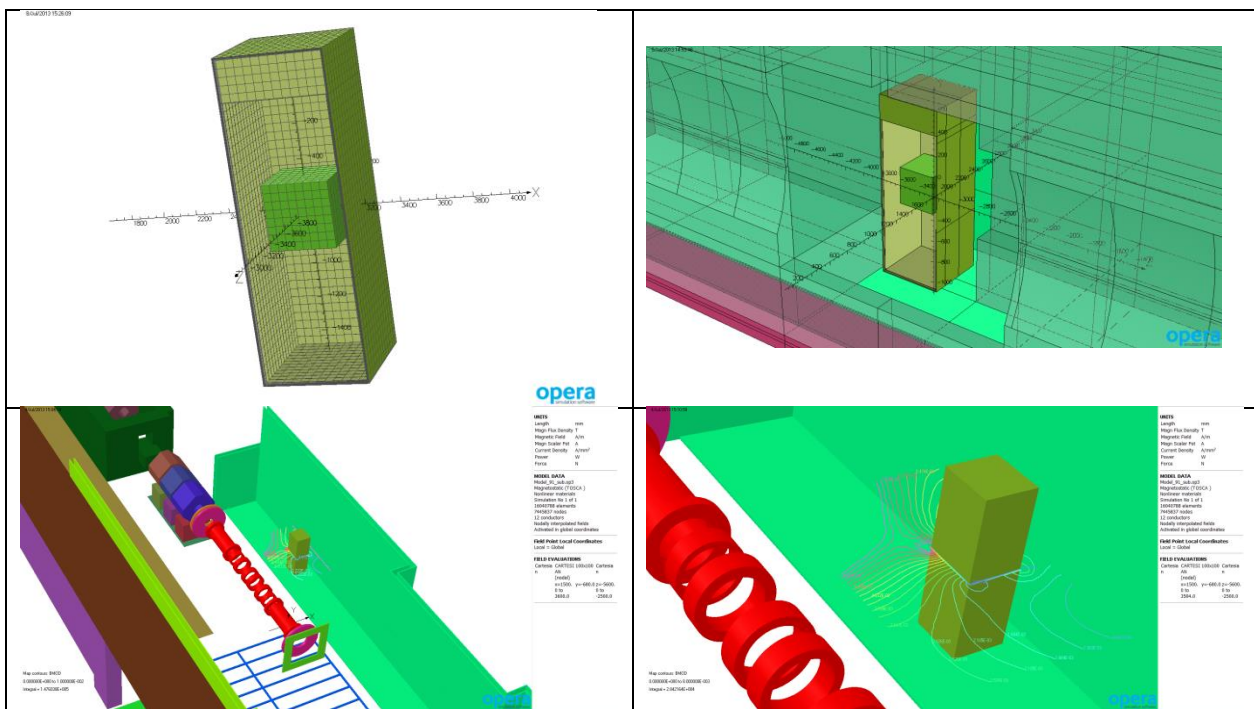


Figure 14: The rack that was extracted from an old model; the rack inserted into model 91; flux lines on a patch through the rack from a model 91 that includes the rack

Also the *rack1.opc* was solved separately as a submodel, driven by a magnetic field that is extracted from Model 91 – see step 1) above. The driving field is shown in figure 15.

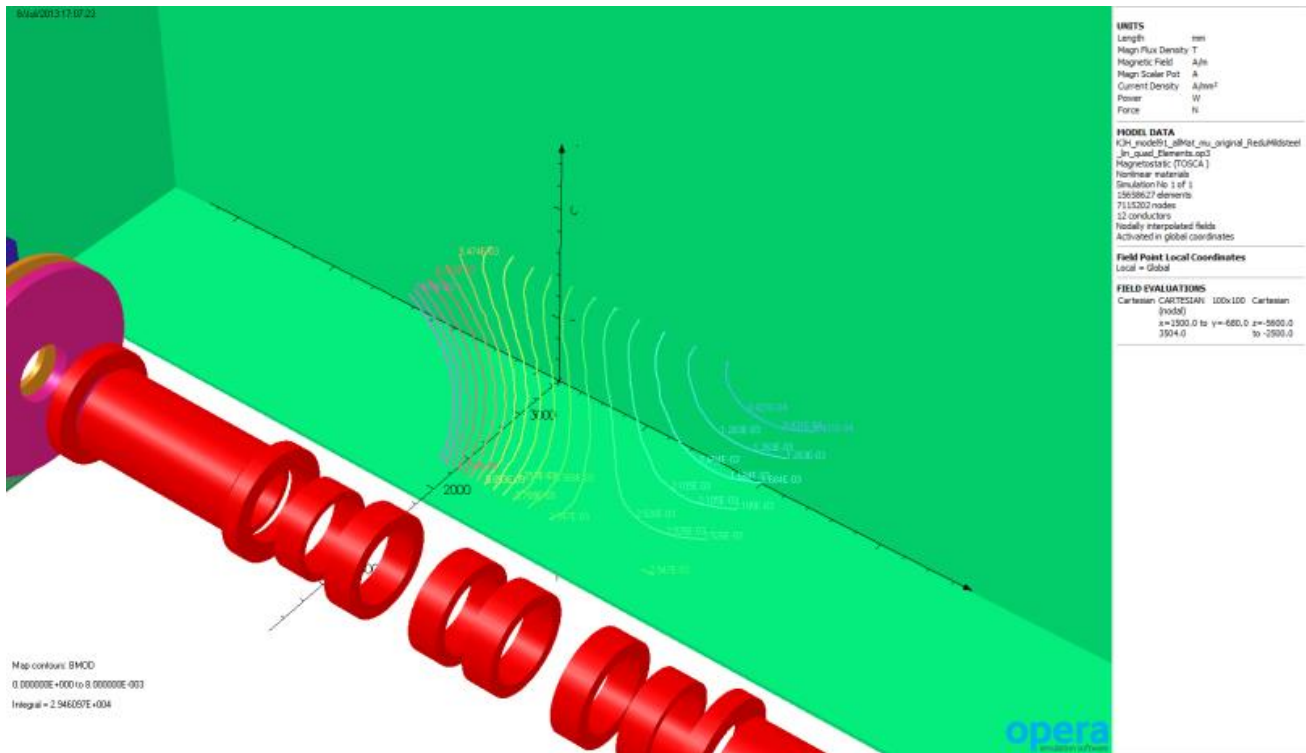
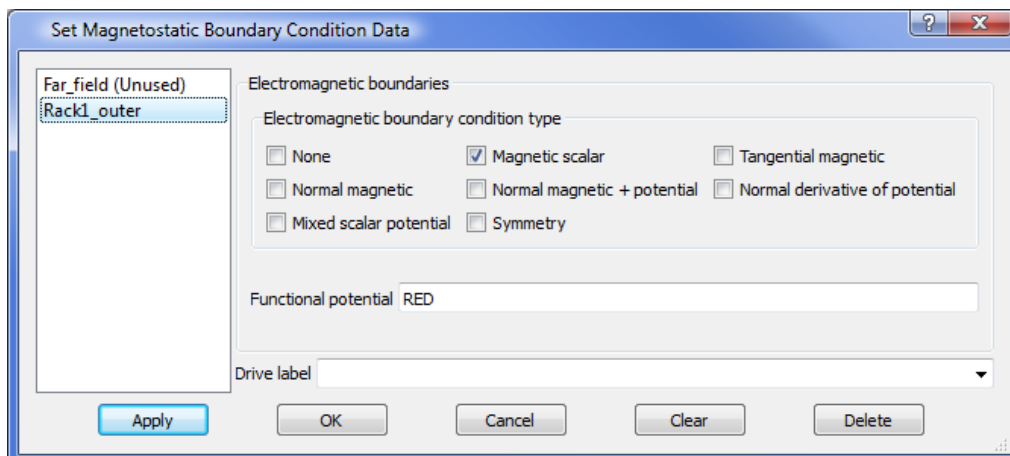


Figure 15: Undisturbed flux lines in model 91 without the rack

The following steps were performed:

1. *Rack1.opc* needs to be surrounded with some elements of air. An air volume was created such that it is as far away as possible from the rack, but does not touch the SSW\_Steel wall. Important is to set the potential type of this air volume to total potential.
2. Select all outer faces of the air volume and specify a boundary condition label. Assign a functional magnetic scalar potential with the name "RED" as shown in the following screenshot:

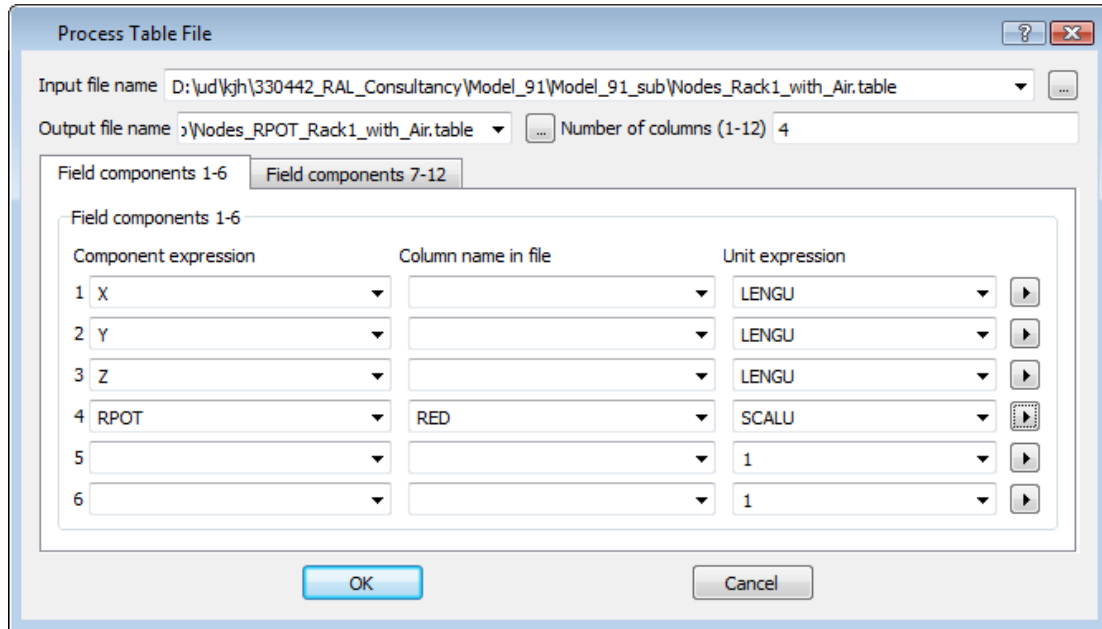


3. Create a database with the name *Rack1\_with\_Air.OP3*, but do not solve it.
4. Load this unsolved model into the Post-Processor and export a table of node coordinates X,Y,Z (nothing needs to be selected for this operation).

**Tables-> Create Table File-> All Node Coordinates**

and chose a filename, for example *Nodes\_Rack1\_with\_Air.table*

5. Load Model 91 (without the rack) into the Post-Processor, process the table of node coordinates and output a new table with columns X, Y, Z and RED as shown below.

**Tables-> Process Table File-> Calculate Fields and save in another Table file**

6. Load the model *Rack1\_with\_Air.OP3* again, and process the new table (*Nodes\_RPOT\_Rack1\_with\_Air.table*) with output to database. This stores the nodal variable RED in the small model.

**Tables-> Process Table File-> Import Fields at all Nodes or Elements**

7. Close the Post-Processor before running TOSCA.
8. Solve the model *Rack1\_with\_Air.OP3* with TOSCA.

## Post-processing and discussion

Inside the rack that is shown in figure 14 there is a green cube. This cube is a bulk material with the name "CompStack2". Figure 16 shows a patch at Y=-680 in the middle of the cube. At this position the direction of the flux is vertical (+By).

For the submodel and for the large model that includes the rack, the integral values of BMOD on the patch were compared.

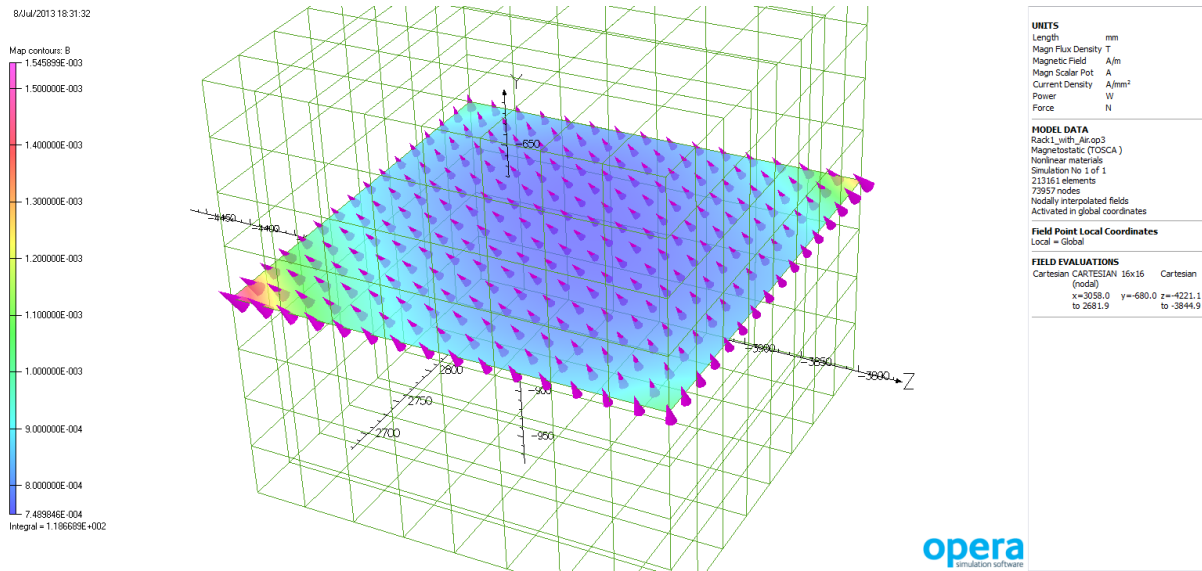


Figure 16: Patch in air that is enclosed in the shielded walls “CompStack2”

Then the integral values of BMOD were compared.

Table 10: Minimum and maximum values of B on patches in [Gauss]

	Integral of B on patch	B min	B max
Large model that includes the rack	69.76 T·mm <sup>2</sup>	4.5 Gauss	10.7 Gauss
Submodel with rack only	118.52 T·mm <sup>2</sup>	7.5 Gauss	15.5 Gauss

Percent error:  $\frac{118.52 - 69.76}{69.76} = \frac{48.77}{69.76} = 69.9\%$

The conclusion is that we get quite a different field distribution in a model with or without a rack. Therefore the field from an overall model not containing that substructure should not be used as a driving field for a detailed sub-model of the substructure.

The other report referred to in the Introduction, “A further investigation of substructure and simplification modelling for the RAL MICE Hall”, shows that substructuring can be more effectively carried out if a simplified model of the substructure is included in the overall model.